





Please cite the Published Version

Gallagher, M, Morden, J, Baker, C, Soper, D , Quinn, A , Hemida, H  and Sterling, M 
(2018) Trains in crosswinds – Comparison of full-scale on-train measurements, physical model tests and CFD calculations. *Journal of Wind Engineering and Industrial Aerodynamics*, 175. pp. 428-444. ISSN 0167-6105

DOI: <https://doi.org/10.1016/j.jweia.2018.03.002>

Publisher: Elsevier BV

Version: Accepted Version

Downloaded from: <https://e-space.mmu.ac.uk/634422/>

Usage rights:  [Creative Commons: Attribution-Noncommercial-No Derivative Works 4.0](https://creativecommons.org/licenses/by-nc-nd/4.0/)

Additional Information: © 2018. This manuscript version is made available under the CC-BY-NC-ND 4.0 license <https://creativecommons.org/licenses/by-nc-nd/4.0/>

Enquiries:

If you have questions about this document, contact openresearch@mmu.ac.uk. Please include the URL of the record in e-space. If you believe that your, or a third party's rights have been compromised through this document please see our Take Down policy (available from <https://www.mmu.ac.uk/library/using-the-library/policies-and-guidelines>)

1 **Trains in crosswinds – comparison of full-scale on-train**
2 **measurements, physical model tests and CFD calculations**

3 M Gallagher, J Morden, C Baker¹, D Soper, A Quinn, H Hemida, M Sterling
4 Birmingham Centre for Railway Research and Education, School of Engineering,
5 University of Birmingham, Birmingham, United Kingdom

6 ¹Corresponding author, e mail c.j.baker@bham.ac.uk

7
8 **Abstract**

9 In this paper a major series of experiments is described that included extensive
10 full-scale measurements of cross wind induced pressures on the Class 43 New
11 Measurement Train over an extended 21 month period, together with wind
12 tunnel, moving model tests and CFD calculations, and allows, for the first time, a
13 proper evaluation of the adequacy of these techniques. Static wind tunnel tests
14 and moving model tests show good agreement with each other, both in terms of
15 the measured pressure field around the train and in the overall side force per
16 unit length over the yaw angle range from 15 to 30°. Similarly the wind tunnel
17 tests and the CFD calculations show good agreement with each other for yaw
18 angles up to 15°. Two different analyses of the full-scale data were carried out -
19 an analysis of one second average wind speeds and forces, and an analysis of
20 specific gusts. There was a very great deal of scatter in the results and only the
21 results from simple track topographies were found to agree well with the model
22 and computational results.

23

- 24 **Keywords** – train aerodynamics, crosswinds, full-scale tests, wind tunnel tests
- 25 moving model tests, CFD

1. Introduction

In the field of railway aerodynamics the main tools that are used in both design and research are physical model testing and computational fluid dynamics. With regard to the former both conventional wind tunnel tests are used (particularly when looking at crosswind behavior eg. Cheli et al 2010) and also moving model tests when looking at transient behaviour both in the open air and in tunnels (eg. Dorigati et al 2015, Sturt et al 2015). CFD techniques have developed significantly in recent years, and although standard RANS techniques are still in regular use (eg. Eichinger et al 2015), more resource intensive methodologies such as DES and LES are increasingly being used (eg. Morden et al 2015).

Now whilst these techniques are relatively straightforward to use, they are based on the fundamental assumption that they are a reasonable approximation to reality, and thus rely on full-scale measurements for their calibration and verification. In the past a number of major experimental full-scale measurements have been carried out to provide fundamental real world data – see Ko et al (2012) for tests on tunnel aerodynamics, the RAPIDE experiments (RAPIDE consortium 2001) and AeroTRAIN experiments (Baker et al 2015) for slipstream and underbody flow measurements, and these have gone some way towards validating the experimental and computational techniques that are used. However when considering the behaviour of trains in the open air with crosswinds of any description, full-scale validation data is less readily available, largely because of the difficulty of the experiments and the need to wait for the correct weather conditions, which can cause major resource issues. Only two tests of this nature are known to the authors. The first was actually a model scale test carried out on a 1/5th scale Advanced Passenger Train in the open air on a

51 test track at Pendine in South Wales (Cooper 1980) – figure 1a. Aerodynamic
52 forces and moments were measured using internal balances and wind conditions
53 were measured with probes mounted on a boom ahead of the model. The results
54 for aerodynamic rolling moment against yaw angle (the wind direction relative
55 to the train) are shown in Figure 1b below, together with some conventional low
56 turbulence wind tunnel results using the same model. The second set of
57 experiments was carried out using a full-scale Inter-Reggio train as part of the
58 TRANSAERO project (Matschke and Heine 2002, figure 1c). Force and moment
59 coefficients were based on the output of force transducers connected between
60 the front bogie and the train body, with an assumption being made as to the
61 point of action of the wind forces, and wind conditions being measured with a
62 long boom in front of the train. Again, rolling moment coefficient values are
63 shown in figure 1d, together with comparative values from wind tunnel tests on
64 an aerodynamically similar ICE-2 train. The two different experiments cover
65 different yaw angle ranges. Both sets of full-scale data lie below the wind tunnel
66 data - for the Pendine tests this is almost certainly due to the differences in
67 ground simulation, and for the TRANSAERO tests the discrepancy may lie in the
68 need to make assumptions concerning the point of action of the aerodynamic
69 forces. There can also be seen to be considerable scatter in the results as might
70 be expected – particular for the Pendine results. The major lesson from these
71 tests is probably that carrying out full-scale measurements of train aerodynamic
72 cross wind forces is very difficult, with many experimental compromises
73 required, even with well defined trains operating on a test track.

74 This paper presents some of the results of a major investigation in which full-
75 scale experiments were carried out to measure cross wind forces and pressures

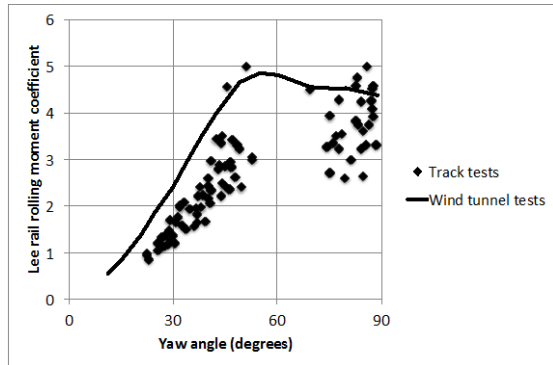
76 on a test train used to measure track characteristics on UK main lines (the New
77 Measurement Train or NMT). These tests were carried out over an extended
78 period of 21 months and large amounts of data were obtained for a variety of
79 wind conditions. Equivalent wind tunnel and moving model rig experiments
80 were carried out for comparison with the full-scale tests, together with similarly
81 equivalent CFD calculations.

82 Section 2 gives details of the various experiments and calculations that were
83 carried out at both model scale and full-scale. Section 3 then describes the flow
84 fields that were measured in the wind tunnel experiments and simulated in the
85 CFD calculations, to give an overall description of the flow around the train.
86 Section 4 then compares the aerodynamic forces and moments that were
87 measured in the physical model tests and the CFD calculations. The full-scale
88 results from the NMT are then considered in detail in section 5, and compared
89 with the results of section 4. Finally some broad conclusions are drawn in section
90 6.

91



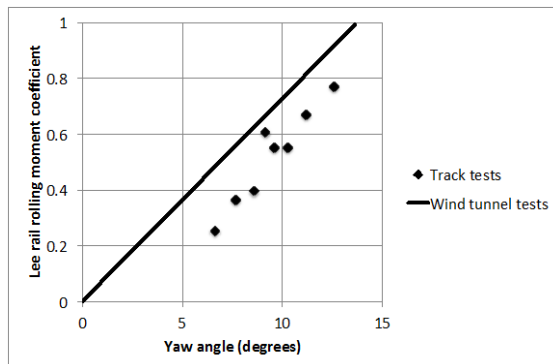
(a) The Pendine experiments using 1/5th scale APT (photograph from National Railway Museum)



(b) Pendine experiments - lee rail rolling moment coefficient results (from Cooper 1980 - redrawn)



(c) The TRANSAERO full-scale Inter-Reggio measurements (author photograph) showing wind measurement boom at front of train



(d) TRANSAERO experiments - lee rail rolling moment results (from Matschke and Heine 2002 - redrawn). Note that the wind tunnel results are not from an identical train and are extrapolated from higher yaw angle values.

Figure 1 Earlier experiments

2. Experimental and computational methodologies

2.1 Definitions

In what follows we will use the definitions of velocities and angles shown in figure 2. Here u is the wind speed, at an angle β to the train direction of travel; v is the train speed, and V is the wind velocity relative to the train. The yaw angle ψ is the angle of this relative velocity to the train direction of travel. V and ψ are give by the equations

$$V^2 = (v + u\cos\beta)^2 + (u\sin\beta)^2 \quad (1)$$

$$\tan \psi = \frac{u\sin\beta}{v+u\cos\beta} \quad (2)$$

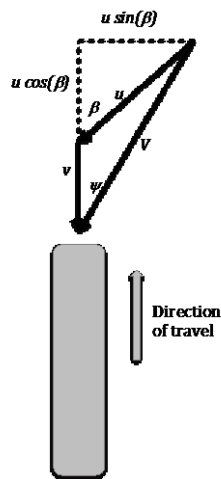


Figure 2 Velocity and angle definitions

2.2 Full-scale measurements

Full-scale measurements were made on the Network Rail New Measurement Train (NMT) – figure 3a. This train, in various formations, runs along every main line in the UK on a thirteen-week cycle to measure track and infrastructure properties using a variety of different types of instrumentation. It consists of two Class 43 power cars (chosen from four that are available) and a variable number of intermediate Mark 3 coaches. Network Rail allowed the University of Birmingham to instrument one of these power cars for aerodynamic measurements for an extended period of measurements between 3/10/2013 and 22/6/2015. This instrumentation consisted of the following components.

- A Pitot tube at the nose of the train (figure 3b) together with three static pressure holes along the front of the train nose (figure 3c). These were connected to a box behind the nose panel containing six pressure transducers. The transducers were connected to the data acquisition system in the luggage compartment near the rear of the power car and pressures p were sampled at a rate of 128 samples / sec.
- A loop of static pressure holes around the sides and roof of the train, 15m from the nose, connected to three pressure transducer boxes, each with five or six transducers (figure 3d). The positions of the tappings are shown in figure 3e. These were again connected to the data acquisition system and pressures sampled at 128 samples / sec.
- A partially sealed reference pressure reservoir within the train itself, to give the reference backing pressures for the transducers p_R . It consisted of an inflexible ceramic pot with a small hole that slowly adjusted the pressure to ambient over a period of about 30 to 60 seconds, which gave a stable

reference pressure against the shorter timescale fluctuations caused by crosswinds and passing trains/tunnels, while still adjusting for variations in altitude. Pressures at two other reference locations were measured in order to correct the first value where necessary - an identical container that was completely sealed to correct for any temperature fluctuations, and an open ended static probe in the luggage area of the power car to correct for any changes in altitude .

- A computer based data storage system, which enabled up to two weeks data to be stored.
- A GPS device, which gave train position and speed every second.

The nose Pitot tube was intended to measure the air speed relative to the train, *V*. Pitot tubes are insensitive to yaw angle for angles of less than about 15 degrees, but it was felt that in normal operating conditions this would only be exceeded very occasionally. Ideally the tube should have been positioned further in front of the train, but the use of an operational train made this impractical and Network Rail stipulated that the probe should not extend beyond the nose of the vehicle. Thus the Pitot tube reading was calibrated against the free stream velocity through wind tunnel tests and a factor applied to convert the measured velocity to free stream velocity. This was not ideal, but was an inevitable consequence of using operational trains.

The pressures from all the taps (on the nose and the loop) were then put into pressure coefficient form

$$C_p = \frac{p - p_R}{0.5 \rho V^2} \quad (3)$$

The nose pressure taps were positioned so as to be able to give an indication of yaw angle ψ . This was obtained by forming the ratio

$$R = \frac{C_{pL} - C_{pR}}{C_{pC}} \quad (4)$$

where subscripts L, R and C refer to the left, right and centre nose tappings respectively. This ratio was also calculated from TRAIN Rig data using pressures measured on the models at equivalent points, and is directly related to yaw angle (see section 2.3 for further details). This calibration curve is presented in section 5 below.

The pressures measured at the side of the train recorded a number of distinct phenomena – the transient pressures due to the passing of other trains; the pressure transients as the train passed through tunnels; and the effects of both steady and transient crosswinds. It is with the latter two sets of data that the present paper is concerned, although a rich database of train passing and tunnel effects has been obtained that will be more fully investigated in the future.

The analysis of the data was complex and is fully outlined in Gallagher (2016). Essentially algorithms were developed to calculate the train speed and direction, identify and remove passing train and tunnel pressure transients from the data; and to apply the calibrations to the Pitot tube and nose pressure tappings to obtain the air speed relative to the train and the yaw angle. Pressure coefficient time histories were calculated for the Pitot tube and each pressure tap.

Two types of analysis were then carried out. Firstly one second averages of train speed, yaw angle and pressure coefficients on the loop around the train were obtained. Only data for which the instrumented vehicle was at the front of the train, train speed was greater than 20m/s, the wind speed was greater than

4m/s and for head wind conditions (i.e. $90^\circ < \beta < 90^\circ$) were then considered, giving a total of 3327 data points. The side force coefficient per unit length was also calculated for each one-second set of data, through integration of the pressure coefficients around the loop (which excludes the underbody pressures). Note that this calculation did not take into account any lateral components of underbody pressures. Gallagher (2016) shows from the wind tunnel data that the difference in side force coefficient around the loop calculated with and without an underbody component was small. This is given by

$$C_S' = \frac{\sum C_{pi} \sin \theta_i A_i}{0.5 \sum \sin \theta_i A_i} \quad (5)$$

where C_{pi} is the pressure at tapping i , A_i is the tributary area for tapping i (with unit width), and θ_i is the angle to the horizontal of the tributary area. Note that the lift force coefficient around the loop was not calculated as no measurements of pressure were made beneath the train.

Secondly, transient wind events were investigated. The wind speed time histories were interrogated and sudden increases in wind speed from near zero were identified. These might be due to the train emerging from a cutting or shelter of some kind into across wind, or from a sudden wind gust. For each identified case the time series of yaw angle, pressure coefficients and side force coefficients per unit length were calculated as above. This process resulted in 220 gust datasets.

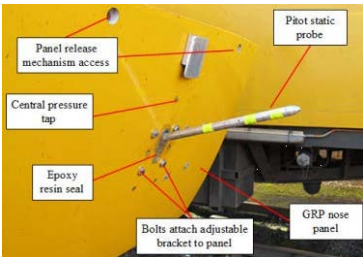
In measurements such as these, it is necessary to consider carefully the possible experimental errors. Gallagher (2016) sets out a full error analysis. In broad terms the possible errors in the values of pressure coefficient for the windward

202 and leeward wall taps are of the order of ± 0.02 to 0.03 , and for the roof taps are
203 of the order of ± 0.04 to 0.05 .

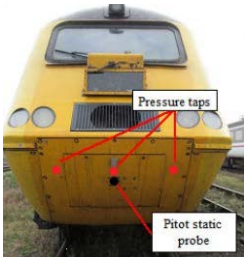
204



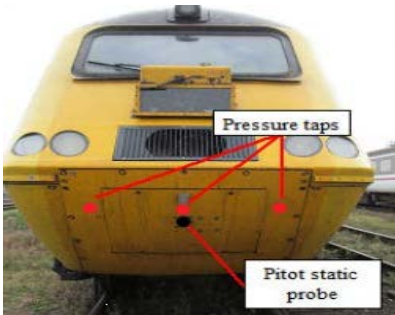
(a) The Class 43 New Measurement Train



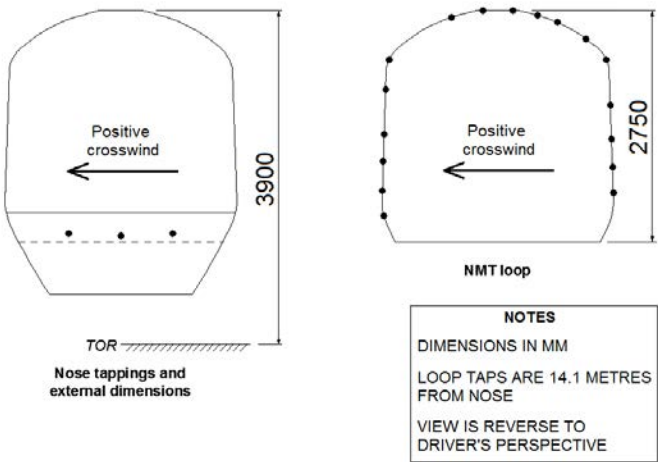
(b) Nose Pitot (on open flap)



(c) Nose pressure taps



(d) Loop pressure taps



(e) Loop pressure tap locations

Figure 3 The Class 43 New Measurement Train

2.3 Wind tunnel tests

Wind tunnel tests were carried out in the RWDI wind tunnel in Dunstable, UK, using a 1/25th scale model of the Class 43 power car and one trailing Mark 3 coach, mounted on ground board, with a “single track ballasted rail” (STBR) representation of the track (figure 4a) – see CEN (2016) for a full specification of the STBR simulation. Pressures were measured on the surface of the model through 313 pressure taps connected to pressure transducers and sampled at 512Hz for 120s (figure 4b). The Reynolds number of the tests, based on vehicle height was 1.4×10^5 (lower than specified by CEN (2016)), and the turbulence intensity of the flow was 5.5%. (higher than specified by CEN (2016)). Note that a further series of tests were carried out with a slightly lower Reynolds number and about twice the level of turbulence intensity, but the results were very similar to the above case and will not be considered further. Full details are given in Gallagher (2016). Pressure coefficients were again formed using the definition of equation (3) with V given by the wind tunnel speed, and p_R by the wind tunnel reference pressure measured at a reference static probe upstream of the train. The surface pressure field was measured at yaw angles between 0 and 50 degrees in five-degree increments. The overall forces and moments on the vehicle were calculated by integration of all the pressure at all theappings. In what follows we will only consider the side force and lift force coefficients which, using the notation outlined above, are given by

$$C_S = \frac{\sum C_{pi} \sin \theta_i A_i}{A} \quad C_L = \frac{\sum C_{pi} \cos \theta_i A_i}{A} \quad (6)$$

where A is a reference side area of 60m². To enable a comparison with the NMT results to be made, the side force coefficient per unit length, C_S' was also

232 calculated at the position of the NMT loop pressure tapplings, using the definition
233 given in equation (5).

234 Finally a full error analysis was carried out and gave pressure coefficient error
235 estimates of ± 0.05 to 0.06 for each pressure tap, corresponding to an error of
236 between 0.02 and 0.07 for lee rail rolling moment coefficient for a yaw angle
237 range between 0 and 45° .

238

239

240

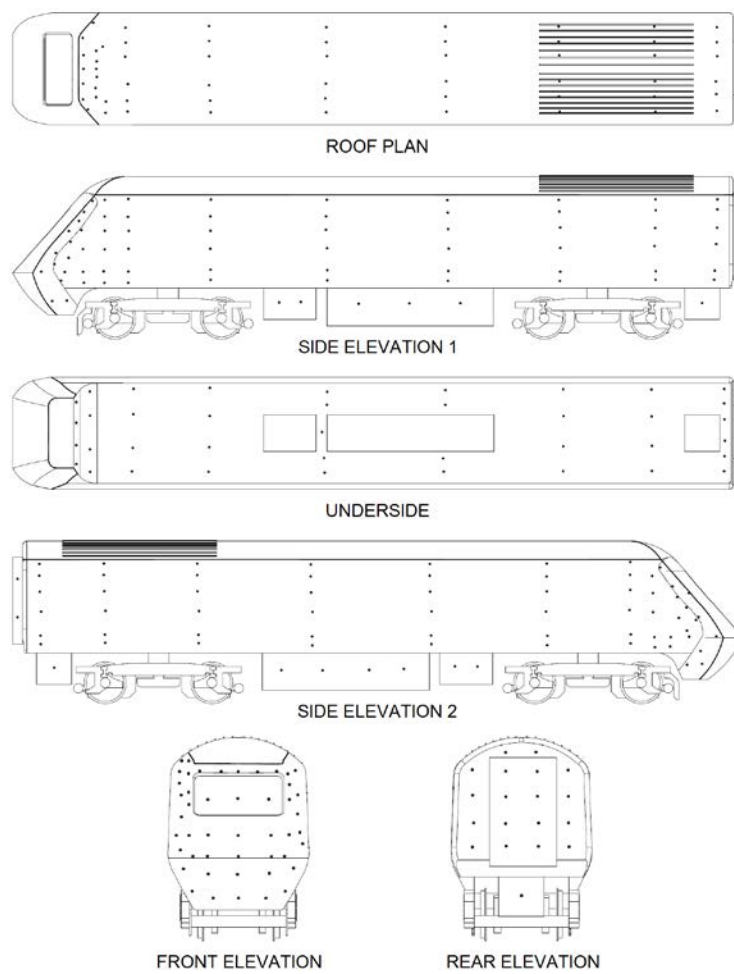


241

242

(a) The wind tunnel model and setup

243



244

245

(b) Tapping positions on wind tunnel model

246

Figure 4 wind tunnel tests

247

2.3 Moving model tests

A series of measurements of train surface pressures in a crosswind was made using the moving model TRAIN Rig and a 1/25th scale model of the Class 43 power car (figure 5a). This rig is fully described in Dorigatti et al (2013). Essentially it consists of two 150m long tracks along which train models can be fired at speeds of up to 75m/s using catapult mechanisms for both firing and braking. It has been used extensively in recent years for train slipstream measurements (Soper et al 2016), underbody flow measurements (Soper et al 2017) and to investigate the generation of sonic booms from tunnel exits (Sturt et al 2015, Vardy et al 2015). For the experiments reported here measurements were made within a crosswind generator, which produced a representation of the natural wind over a 6.4m length of the track (figure 5b). The geometry of the rig is such that it is constrained laterally (by operating railway tracks either side of the building which houses it) and thus there is little development length for the crosswind generator. Nonetheless the flow quality is acceptable for the experiments that are presented here, although the velocity varied by up to 10% along the length of the generator. The maximum average wind speed in the generator was 12m/s, with longitudinal, lateral and vertical turbulence intensities of 0.2, 0.1 and 0.1 respectively, and a longitudinal length scale of 0.4m model scale. Full details of the flow field characteristics are given in Dorigatti (2013) and Gallagher (2016).

Pressures were measured on the surface of the model at the position of the loop on the NMT (figure 5c) at 0.8 of the vehicle length from the nose, and at the pressure ports on the train nose. The technique adopted was the same as that described in Dorigatti, with the static pressure holes being connected to 15

pressure transducers mounted within the model (figure 5d). A light sensor was housed on the leeward sidewall of the train model and four external lasers were spaced across the length of the test section in order to calculate train speed and deceleration. Data acquisition systems, batteries and a reference pressure reservoir were also mounted within the model itself, and the pressure data was downloaded via a USB port after each run. Track based measurements were aligned with the on train measurements using a train based light sensor that detected a beam of light at a fixed point on the track.

Tests were carried out at 15, 20, 25 and 30 degrees yaw, with the crosswind generator speed being kept constant and the vehicle speed being changed to obtain the correct yaw angle. The Reynolds number thus varied between 2.3 and 4.5×10^5 . For each yaw angle 15 runs of the rig were required to obtain stable pressure averages. All pressures were expressed as coefficients using the formulation of equation (3). The nose pressure measurements were used to obtain a yaw angle calibration for the full-scale NMT experiments (see below) and the loop pressure measurements were used to analyse the effects of cross winds, with side force coefficients per unit length being formed (equation (5)).

An error analysis gave potential errors for the leeward face pressures of ± 0.05 to 0.06, for the roof of ± 0.04 to 0.05 and for the windward wall of ± 0.025 to 0.035.

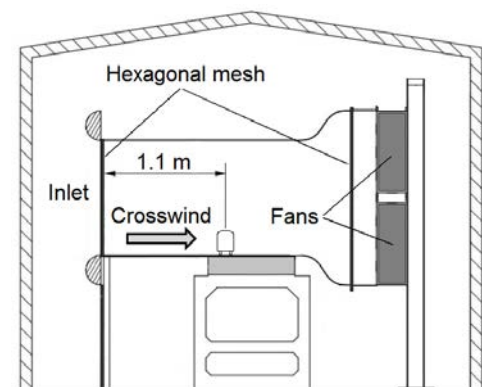
Errors in side force coefficient per unit length were of the order of 0.02 over the yaw angle range considered.

295

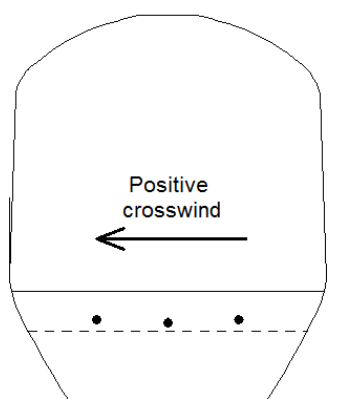
296



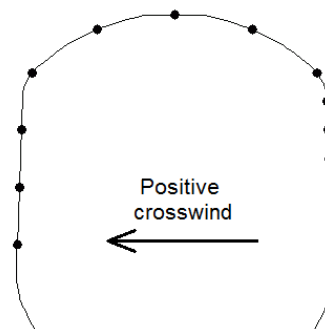
(a) Train Rig model



(b) Crosswind generator (from Dorigati et al 2013)



TOR
Nose taps and
external dimensions

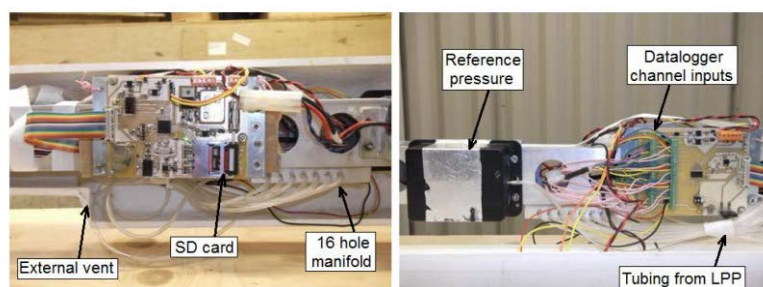


TRAIN rig loop

NOTES

LOOP OF TAPS IS 565 MM FROM NOSE TIP
AT MODEL SCALE
VIEW IS REVERSE TO DRIVER'S
PERSPECTIVE

(c) TRAIN Rig model pressure tap positions



(d) TRAIN Rig model internal arrangement showing pressure tap manifold, data logger and reference pressure reservoir

Figure 5 The Moving model experiments

2.4 CFD simulations

CFD calculations were carried out around a 1/25th scale four-car model – two Class 43 power cars with two Mark 3 carriages between them - and are fully reported in Morden (2016). Three sets of calculations were carried out – to simulate the zero yaw angle results obtained in the wind tunnel; to simulate the slipstreams around the model for comparison with full-scale results and TRAIN Rig slipstream measurements; and to simulate the crosswind measurements that were also made at the TRAIN Rig. It is the latter that is under consideration here. Note that the calculations were carried out using a four-vehicle train similar to the work of Gallagher (2016).

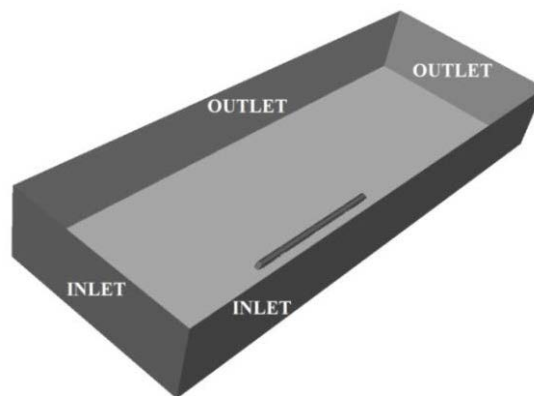
Calculations presented in this paper were carried out using the OpenFOAM software (OpenFoam 2015) using the DDES approach. The DDES approach used in this investigation is detailed in Morden et al (2015).

The domain used is shown in figure 6a below. The length of the domain is 44H (where H is the model height), the height is 9H, and the width is 24H, 6.5 H on the windward side of the domain and 17H on the leeward side. Similar to the wind tunnel tests the inlets, at the front and on the windward side of the domain are taken as constant velocity boundaries, and the outlets at the end of the domain and on the leeward side are taken as constant pressure boundaries. All the boundaries of the train model are specified as no-slip, whilst the ground, track and roof boundaries is specified as slip boundaries. The inlet velocity at the front of the domain is kept constant whilst the inlet velocity normal to the windward side of the domain boundary is varied in order to simulate different yaw angles. This is the other way round to the TRAIN Rig measurements, but was more practical in terms of the mesh set up that was used.

A number of meshes were developed for the various investigations. For the crosswind comparisons reported here two were used - the medium mesh with 40.3m cells, and the fine mesh with 74.5m cells. Figure 6b shows details of the mesh, including details of the refinement region that extended 5H ahead of the model, 48H behind the model, 7H from the top of rail above the model, 2H from the centre of the track on the windward side and 8H from the centre of track on the leeward side. A further refinement region was defined very close to the train, that extended 1.5H ahead of the model, 30H behind the model, 1.5H from the top of rail above the model, 1H from the centre of the track on the windward side and 2H from the centre of track on the leeward side.

Grid sensitivity tests were carried out at ten degrees yaw angle, and the side and lift force coefficients for the two meshes are shown in table 1 below. There can be seen to be little difference between the results of the two meshes, and thus the medium mesh was used to produce the results that are presented below.

337

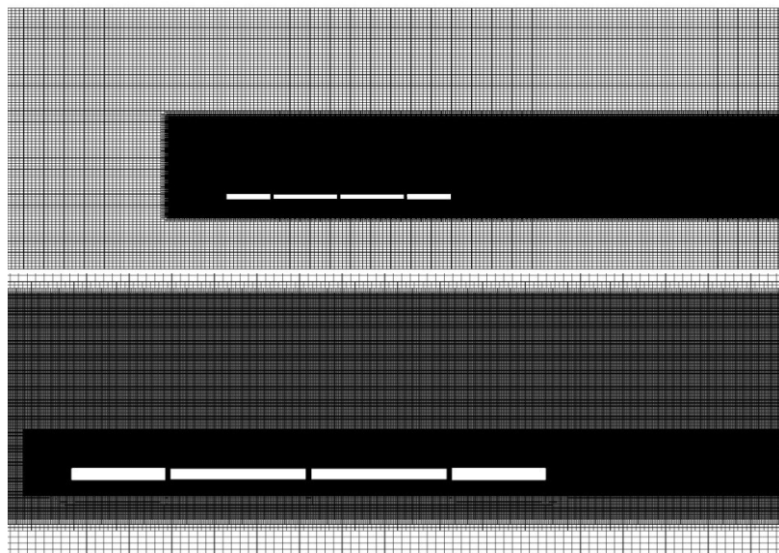


338

339

(a)]The calculation domain

340



341

342

b) The grid, showing the two refinement regions

343

344

Figure 6 CFD calculations

345

346

Table 1 Mesh sensitivity check at a yaw angle of 10 degrees

	C_s	C_L
Medium	0.528	0.059
Fine	0.521	0.059

347

348

2.5 Yaw angle ranges

Each of the experimental and computational methods that were used in this investigation had limitations on the yaw angle range that could be considered. The yaw angles for the full-scale tests were of course limited by the wind conditions at the time of measurements, and hardly ever exceeded 15 degrees. The wind tunnel experiments were the least restricted in yaw angle terms, but were limited to angles below 50 degrees, as it was known in advance there would be no high yaw angle data for comparison. The TRAIN Rig measurements were limited by the speed of the Rig as it was required to keep the simulated cross wind conditions constant. In effect for low yaw angles high rig speeds were required and for low yaw angles low cross wind speeds. There are limitations on both of these – at high model speeds the rig firing mechanism becomes progressively more unreliable and difficult to use, and at low wind speeds it is difficult to obtain repeatable model velocities from run to run. Thus results were limited to yaw angles of between 15 and 30 degrees in five degree increments. Even here it will be seen that it was not always possible to obtain full data sets because of experimental issues. Finally, the CFD calculations were limited to runs at 5, 10 and 15 degrees, simply because of resource issues in the context of the wider investigation.

3. Flow field description – wind tunnel tests and CFD calculations

Each of the experimental and computational methods that have been adopted in this study have their own particular strengths and weaknesses. A major advantage of the CFD methodology is the ability to visualize the entire flow field around the train model. Figures 7 shows visualisations for the velocity and vorticity fields for the four yaw angles studied – 0, 5, 10 and 15°. Figure 7a shows three-dimensional views of velocity (normalized with train velocity and figure 7b shows iso-surface of the second invariant of the velocity gradient tensor, Q . The positive values of Q indicate regions where the vorticity magnitude is greater than the rate of strain in the flow and thus flow vortices exist. The development of inclined vortex structures in the wake can clearly be seen in both figures. Such structures were first observed by Mair and Stewart (1985), and form the basic flow pattern around high speed trains at low yaw angles in low turbulence conditions. Figure 8 shows horizontal (figure 8a) and vertical (figure 8b) cross section plots of velocity and pressure contours, showing the low-pressure region in the lee of the train nose and in the centre of the vortex wake at the higher yaw angles. The velocity contour plots at 10m from the train nose (figure 8b) show that the flow is attached over the roof of the train, although there is very low pressure over the train roof at the higher yaw angles. The complex, high velocity flows on the leeward side near the ground are also very clear and show multiple centres of vorticity.

The wind tunnel results allow a visualization of the surface pressure field over a wider yaw angle range than the CFD results, and this is shown in figure 9 for yaw angles of up to 50°. As the yaw angles increase it can be seen that the high pressures on the windward walls and the suction over the roof become gradually

stronger. The suction occurs first at lower yaw angles around the nose, but then spreads along the entire length of the train body.

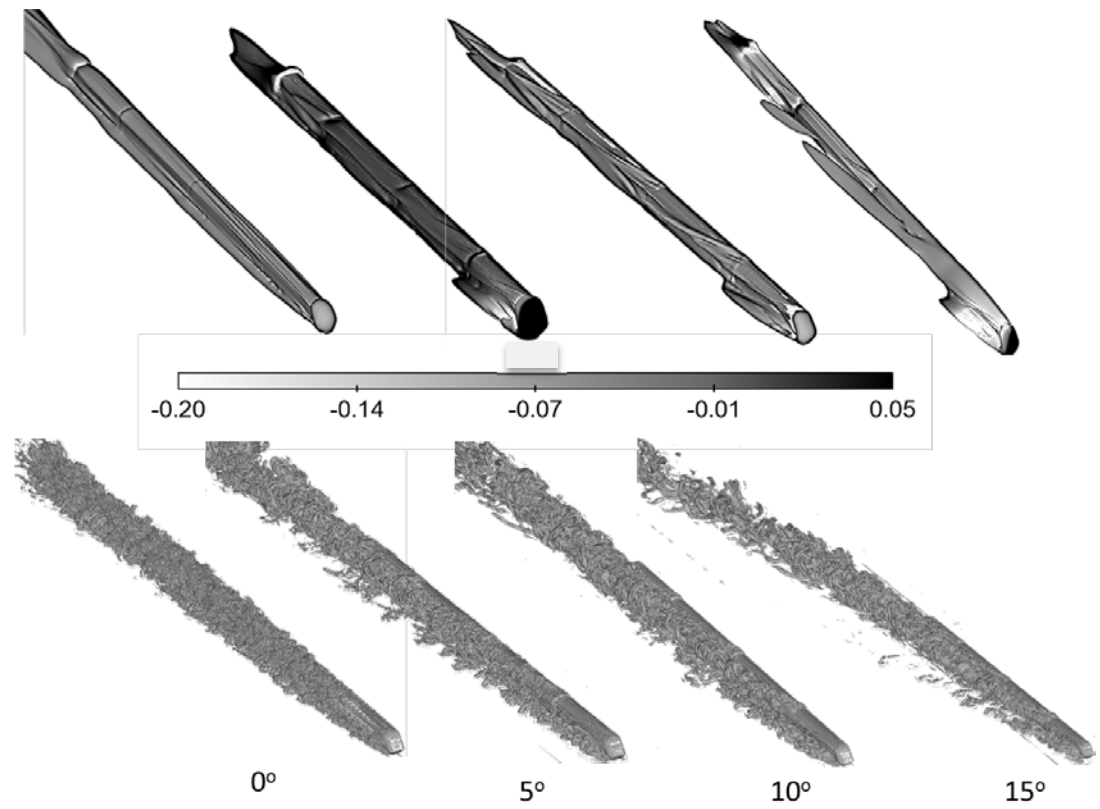
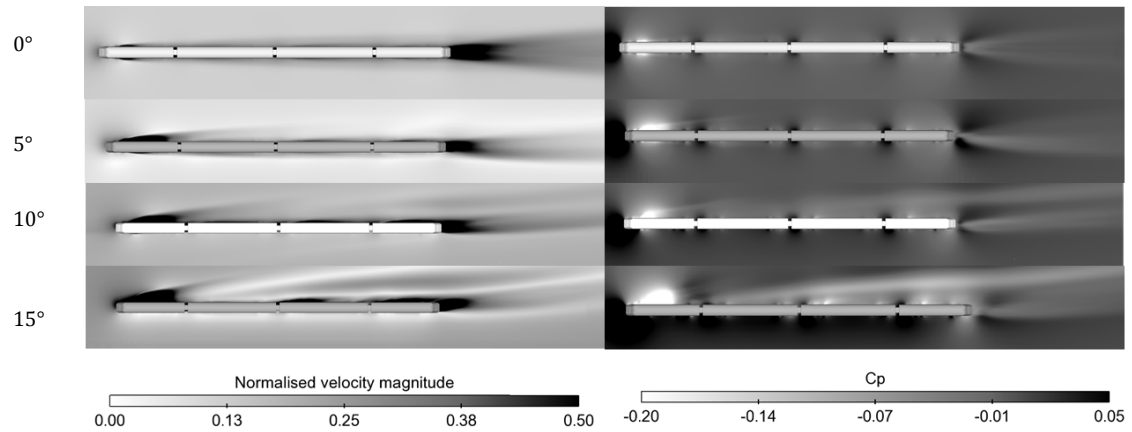
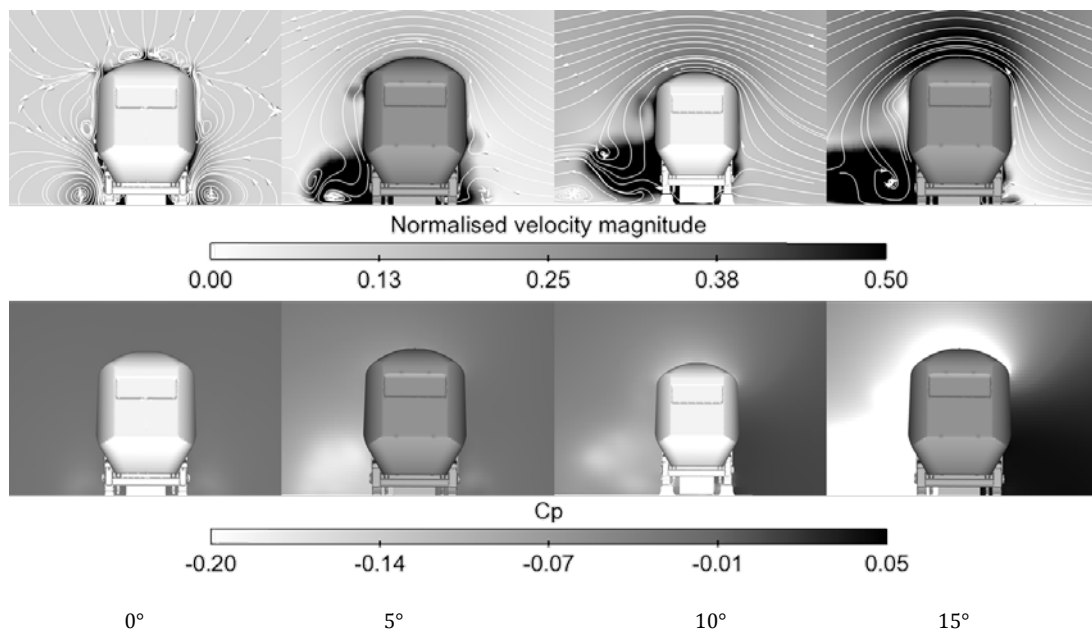


Figure 7 CFD calculations of iso-surfaces of normalised velocity above 0.25 (top row) and second invariant of velocity gradient at $Q=10000$ (bottom row)



(a) Cross section 0.2m above TOR - contours of velocity (left) and pressure (right), showing development of inclined vortex wake as yaw angle increases – above the train in the figures



(b) Cross section 10m from nose - contours of velocity and pressure. The high velocities in the developing trailing vortex wake (on the left of the train profile) can be clearly seen as can the low pressure in the wake and over the top of the train.

Figure 8 Velocity and pressure contours

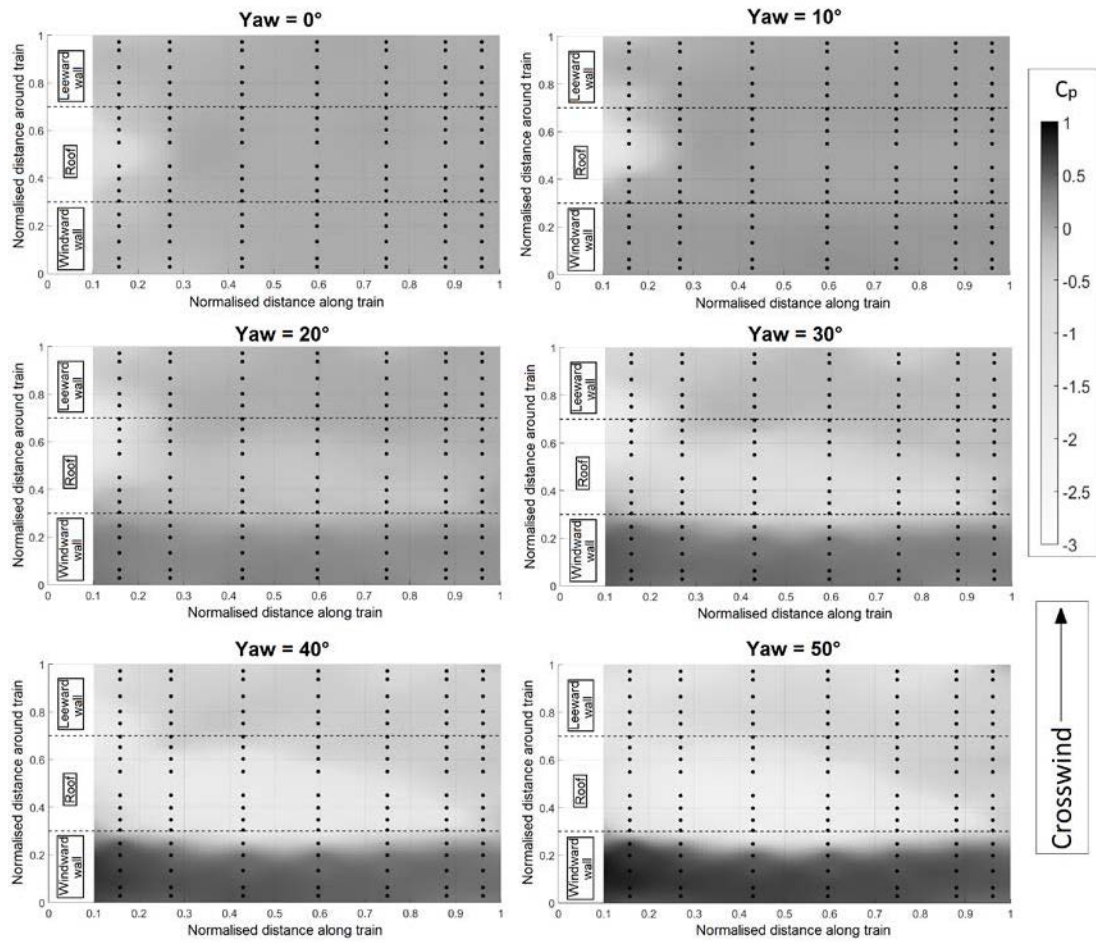


Figure 9 Crosswind pressures on train surface from wind tunnel results.

4. Pressure and force coefficients from wind tunnel and TRAIN Rig model tests and CFD calculations

Figure 10 shows a comparison of the pressure coefficients for the wind tunnel, TRAIN Rig and CFD results for yaw angles of 5, 10, 15, 20, 25 and 30° for the position of the pressure taps on the NMT. Wind tunnel results are available at all yaw angles, CFD results for angles of 5, 10 and 15° (which were chosen to best match the NMT test range and to use the computer resources available to the best effect), and TRAIN Rig results for angles of 15, 20, 25 and 30°. With regard to the latter, it is not possible to measure lower or higher yaw angles on the TRAIN rig, in the former case because this would require low cross wind speeds for which the flow quality was poor, and in the latter case because this would require low vehicle speeds which had poor levels of repeatability. Note that complete results for the TRAIN Rig experiments are only shown for 20 and 25° yaw – for the other yaw angles experimental difficulties resulted in no data being collected for a number of pressure taps. In these figures, the values for the distance of less than 2.5m are on the leeward side of the train, and the values above 5.5m are on the windward side of the train, with the roof taps in the intermediate region.

The agreement between the results can be seen to be extremely encouraging, particularly when the error limits outlined in section 2 are considered. The developing suction peak over the windward roof of the vehicle can be seen as yaw angle increases.

These surface pressures then enable the overall force coefficients to be obtained through integration over the surface. The results for side and lift force coefficients are shown in figure 11. The wind tunnel and CFD results can be seen

to be in reasonably good agreement (with the exception of the lift force at the highest CFD yaw angle). Also shown is a best-fit line of the form suggested by Baker (2013)

$$\frac{C_s(\psi)}{C_s(40)} = \left(\frac{\sin(\psi)}{\sin(40)} \right)^n \quad (7)$$

Here the best-fit value of n was found to be around 1.3. This is typical of blunt ended trains. At first sight this might appear surprising as the Class 43 front end has a streamlined appearance. Nonetheless it also has quite sharp edges, which presumably cause local separations and effectively make it aerodynamically blunt. The value of the coefficients at 40° are also within the range of the trains studied by Baker (2013).

Figure 12 shows a comparison of the side force per unit length around the loop at the position of the pressure taps on the NMT, for the wind tunnel, TRAIN Rig and CFD results. Note that these do not contain any contribution from the flow beneath the train, but for side force coefficients, as noted above, the analysis of Gallagher suggests that the effect is small. It can be seen that there is good agreement between the results of the different techniques. The TRAIN Rig results are restricted to yaw angles of 20° and 25° for the reason set out above. The absolute values of the results per unit length are somewhat below the absolute values for the overall results. As both sets of results are based on a representative side area (60m^2 for the overall results and the body height multiplied by 1.0m for the results per unit length) this implies that the contribution to the overall force coefficient by the loop around which the measurements have been made is less than the average. This is not unexpected, as the suction peak shown in the flow visualisations in the nose region indicates

that this region will be producing a greater force per unit length than the region around the NMT loop.

Thus it can be concluded that the two physical modeling techniques and the CFD calculations produce results that agree well with each other. In the next section, where we move on to consider the NMT results, for the sake of clarity, we will only compare these with the wind tunnel results.

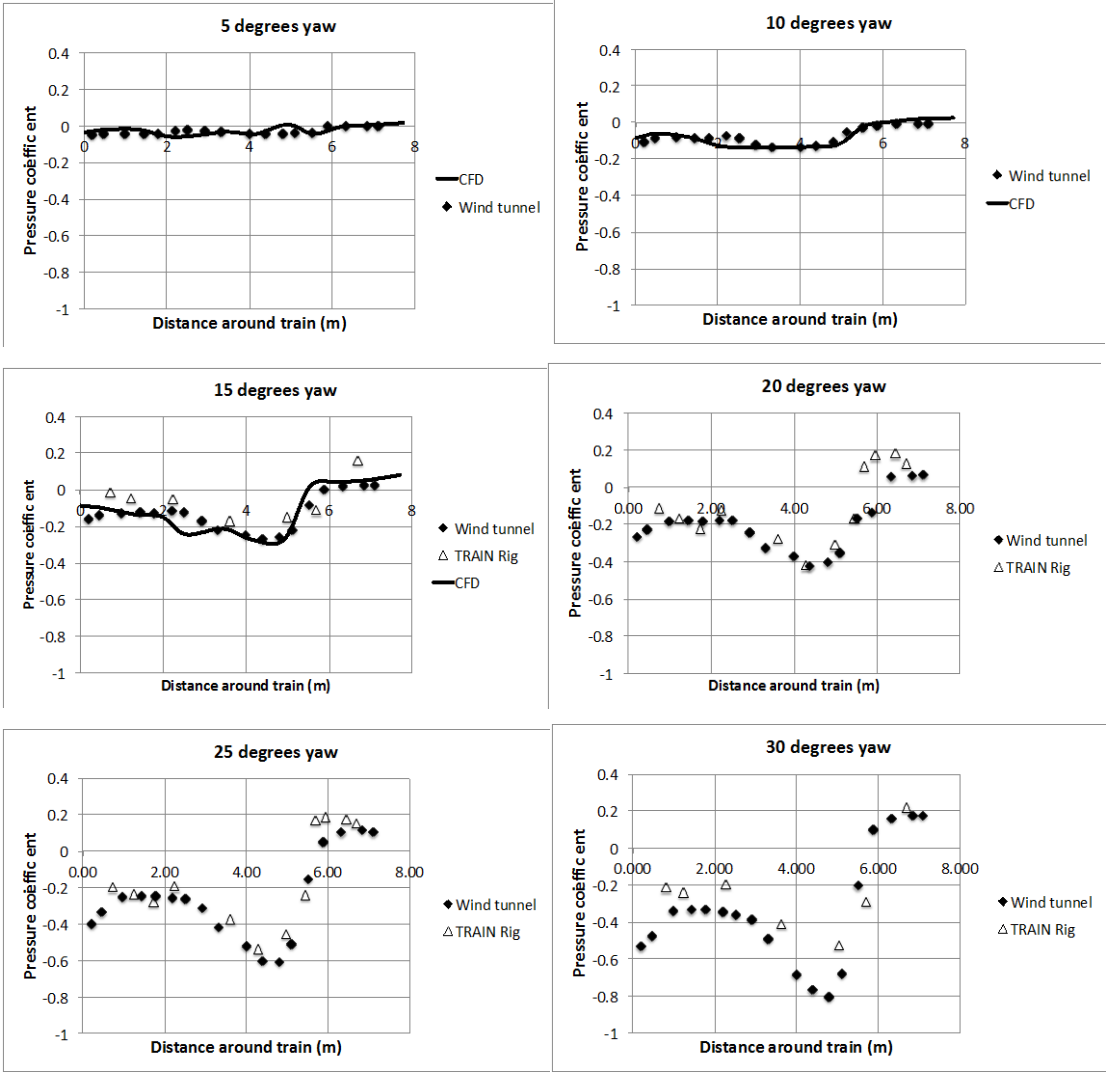
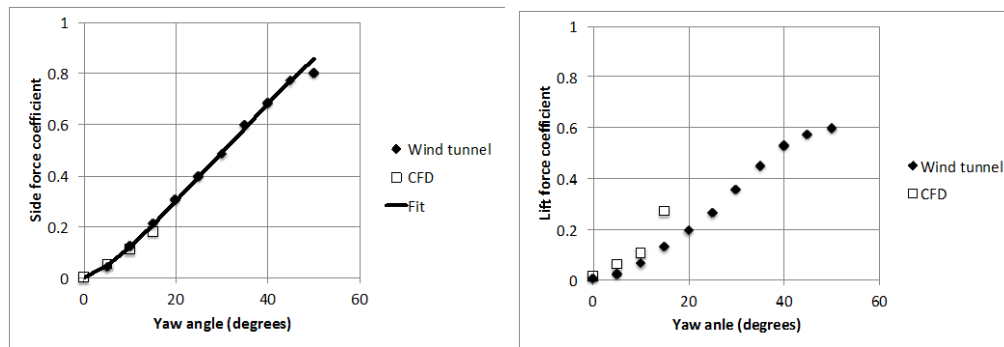


Figure 10 Surface pressure coefficients around the train at the position of the NMT pressure taps (0 to 2.5 – leeward wall; 2.5 to 5.0 roof; 5.5 to 8 – windward wall)

467



468

469

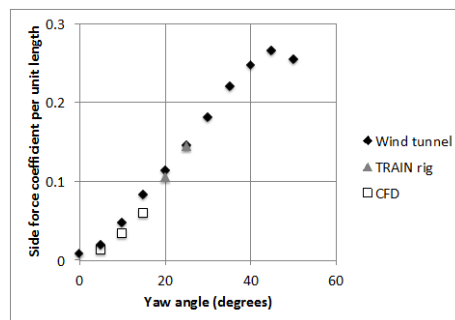
470

471

472

473

Figure 11 Side and lift force coefficient results from wind tunnel measurements and CFD calculations (the dark line shows the fit of equation (7))



474

475

476

477

478

Figure 12 Side force coefficient per unit length from wind tunnel and TRAIN Rig measurements and CFD calculations

5. Force and pressure measurements from the NMT experiments

5.1 Calculation of yaw angle

As set out in section 2, the use of an operating train to obtain the full-scale measurements inevitably meant that some compromises on instrumentation were required. Firstly the Pitot tube at the front of the train could not extend beyond the nose of the train for safety reasons. This probe position was thus calibrated in a wind tunnel, and a correction factor to give the air speed relative to the train V of 2.1 was obtained. This was found to be constant with yaw angle up to 15 degrees, and was confirmed by a comparison of the full-scale train velocity using this calibration and the GPS velocity over a wide range of train speeds (Gallagher (2016)). Also the use of a Pitot tube for the determination of air velocity restricts the results to yaw angles of $\pm 15^\circ$. It will be seen below that all the results obtained fell well within this yaw angle range. Secondly the yaw angle was obtained from a calibration based on the nose pressure taps, in which the parameter R defined in equation (4), was related to yaw angle ψ . This calibration was found from the TRAIN Rig experiments (as these were felt to be more realistic in this regard than the wind tunnel measurements due to the better vehicle / ground simulation) and was given by the equation

$$\psi = 5.28R^3 - 15.01R^2 + 33.77R \quad (8)$$

Note that this calibration was obtained for yaw angles of greater than 15 degrees, and extrapolated to lower yaw angles – an obvious mismatch with the Pitot tube results. Similar measurements in the wind tunnel, over a yaw angle range from 0 to 30 gave a calibration that was identical in form to equation (8) although with different numerical values, which gives some confidence in the

low yaw angle range. The yaw angle values thus obtained will be used in the two analyses that follow – for one-second gusts and for transient gusts.

Once ψ and V have been determined, the wind speed u and wind direction β can be calculated from figure 1 as

$$u^2 = V^2 + v^2 - 2Vv \cos(\psi) \quad (9)$$

$$\tan(\beta) = \frac{V \sin(\psi)}{V \cos(\psi) - v} \quad (10)$$

5.2 Analysis of one-second average values

As outlined in section 2, one-second values of yaw angle and surface pressure coefficients were thus obtained for the following conditions.

- the instrumented power car leading;
- train speeds v of greater than 20m/s;
- head wind conditions only (i.e. $-90^\circ < \beta < 90^\circ$);
- wind speed u greater than 4m/s.

This gave a total of 3327 samples from the 21-month experimental period. The location of these points obtained from the GPS co-ordinates are shown in figure 13, and they can be seen to have been obtained at a wide range of locations across the Great Britain railway network. The range of train speeds, wind speeds and wind directions are also shown. In what follows we will first consider the side force coefficient per unit length, and will then look in more detail at the pressure coefficients around the measurement loop. As all the experimental and computational results are similar, for clarity comparisons with the NMT data will only be made using the wind tunnel results.

Firstly however it should be remembered that the data that was obtained came from a train under normal operating conditions i.e. not on a test track. As such it

will have experienced a wide range of wind conditions, particularly in terms of atmospheric stability, wind speed and turbulence intensity and length scale. Data will also have been obtained for a range of track topographies – on embankments and in partial or full cuttings; in rural and urban environments and so on. Also the one-second data can represent both equilibrium and transient situations, and the flow around the train may be in either a developing or equilibrium state. Thus the data cannot be expected to be clean, but it does nonetheless represent an operational reality.

Figure 14 shows a plot of the side force per unit length against yaw angle for all measured data. Most of the results can be seen to be general consistent with the wind tunnel results, but there is a large scatter in the results. Whilst some of this may be due to experimental methodology (Pitot tube and yaw angle calibration in particular), the scatter is reminiscent of that shown in figure 1 for the Pendine and TRANSAERO experiments, and that found in many full-scale studies of wind loads on buildings and road vehicles (see Richards et al (1995), Quinn et al (2008)) and reflects the unsteady and complex nature of real world flows around trains, due to atmospheric unsteadiness and due to the transient nature of these flows, with overall forces being transient in both temporal and spatial terms and not fully coherent across the train. This point will be discussed further below.

That being said, there is also a possible systematic bias to the data – in particular the positive values of the side force coefficient per unit length for negative yaw angles in the top left corner of the graph. The GPS locations of these data points were investigated individually, and the large majority were found to be at locations where there was a barrier of some sort on the leeward side of the train – trees, cutting side etc.. Because trains in the UK generally run on the left, this

was always on the left hand side of the track in the train direction of travel. When the flow was from the right side of the track (by convention a negative value) the leeside sheltering seems to have resulted in a small side force in the direction opposite to the wind direction. Whilst this data may be regarded as spurious, it is nonetheless a real effect experienced by trains in operational conditions.

In order to investigate the effect of the data sampling criteria used above, the data was analysed for different train velocity, wind velocity and wind direction cut off conditions. Assessing the effects of these changes is not wholly straightforward as the scatter in the data is likely to have a random component due to environmental conditions and a deterministic component due to track topography as outlined above. As a surrogate for the overall random scatter we use the standard deviation in side force coefficient per unit length for yaw angles between 4° and 6° . The sensitivity of this parameter to the sampling conditions is shown in table 2 below. It can be seen that as the train velocity cutoff is increased, the standard deviation falls, particularly in the higher speed range (although note there is also a fall in the number of samples). The standard deviation does not fall however as the wind speed cut off is increased, and reducing the wind angle range actually causes an increase in standard deviation. This rather simplistic analysis suggests that at least the random component of scatter is primarily due to local wind fluctuations, as these will have less effect on the side force coefficient values as the train speed increases. On the basis of this result, a 50m/s lower train speed has been applied to the complete dataset, and the variation of side force coefficient per unit length with yaw angle is shown in figure 15. The number of data points has been reduced to 258. The

variation with yaw angle can be seen to be much more clearly defined and close to the wind tunnel test results, although the positive values of coefficient at negative yaw angles can still be seen.

The average pressure coefficients for all the data are compared with the wind tunnel data for yaw angle bands of $4^\circ < \psi < 6^\circ$ and $8^\circ < \psi < 12^\circ$ in figure 16a (denoted as the 5° and 10° cases respectively) and $-4^\circ > \psi > -6^\circ$ and $-8^\circ > \psi > -12^\circ$ in figure 16b (-5° and -10° cases). These ranges were chosen to give a reasonable number of data points in each range. The NMT data is shown with the mean values and the average standard deviation is also shown as vertical bars. There can be seen to be reasonable agreement between the two data sets, particularly when the full-scale standard deviations, and the errors outlined in section 2 are taken into account. The major deviation is around the windward roof edge, where there the NMT values have a consistently higher magnitude than the wind tunnel values.

592

593

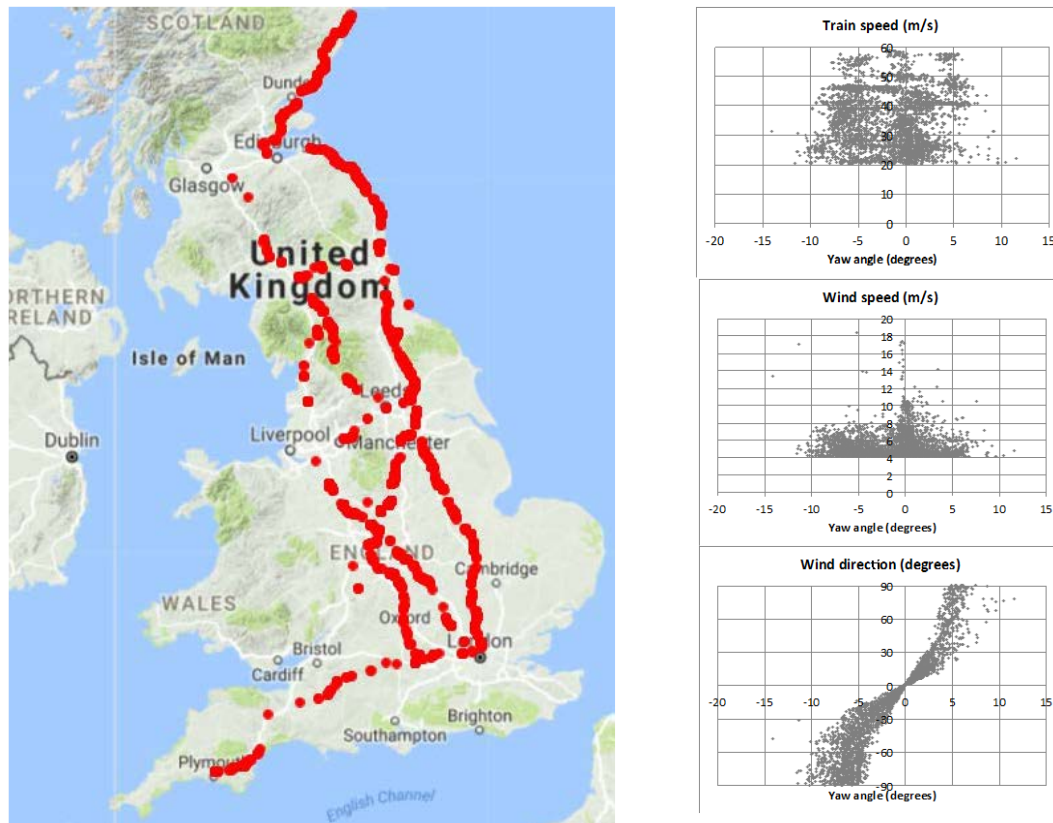


Figure 13 NMT one second average measurement locations and conditions
(train speed cut off of 20m/s; wind speed cut off of 4m/s)

594

595

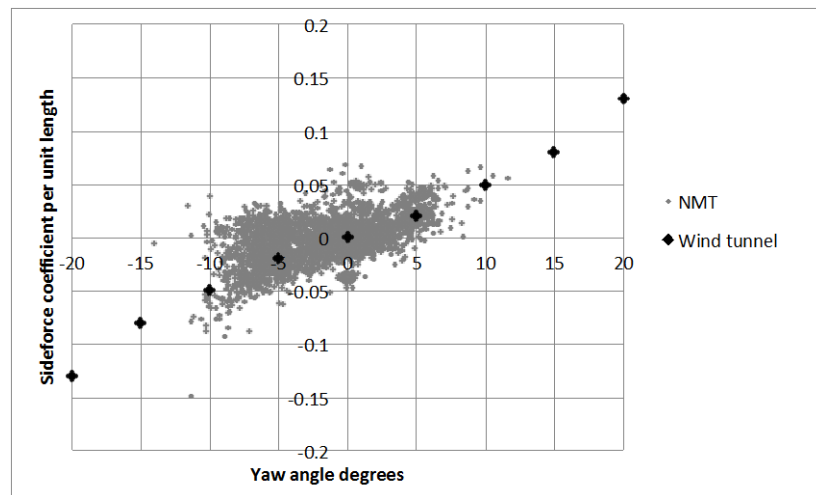


Figure 14 NMT side force coefficient per unit length against yaw angle (all data)

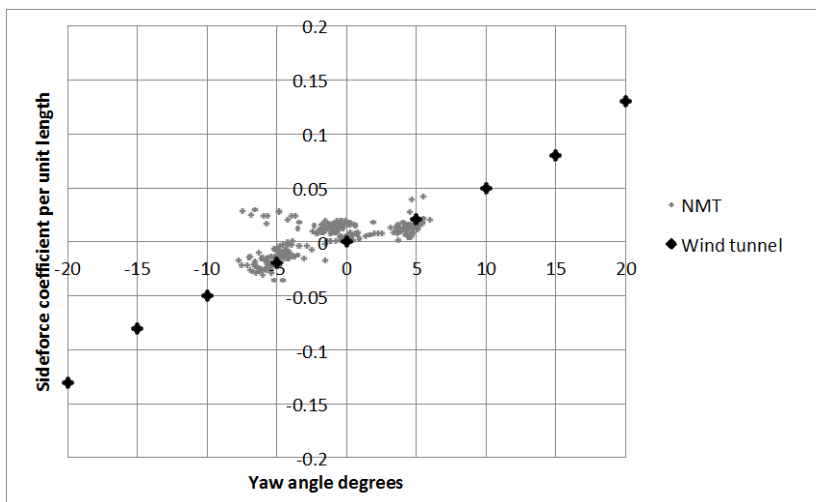
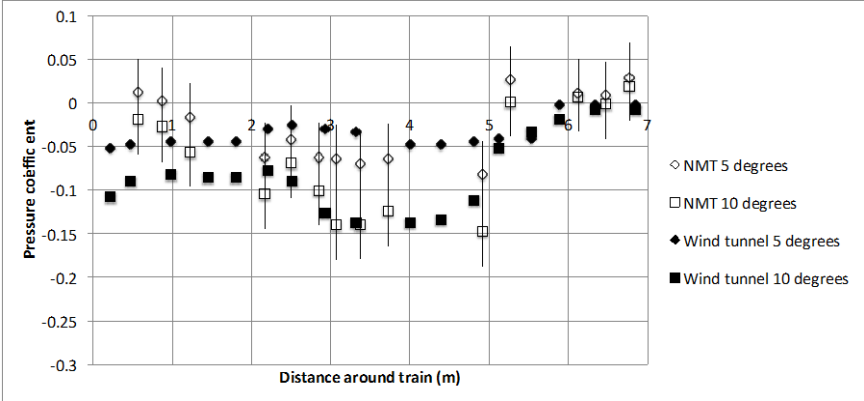


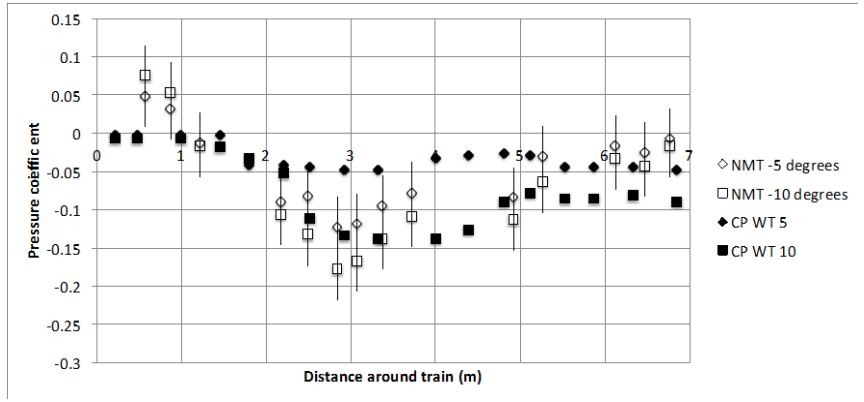
Figure 15 NMT side force coefficient per unit length against yaw angle ($v > 50 \text{ m/s}$)

604



605
606
607
608

a) 5 and 10 degrees yaw - 0 to 2m leeward side, 5 to 7m windward side



609
610
611
612
613
614
615
616
617
618
619
620
621

b) -5 and -10 degrees yaw - 0 to 2m windward side, 5 to 7m leeward side

Figure 16 Pressure coefficients around NMT loop and comparison with wind tunnel data (vertical bars show average standard deviation of all data for that yaw angle)

Table 2 Effect of sampling parameters on standard deviations of side force coefficients per unit length for yaw angles between 4° and 6°.

v (m/s)	20	30	40	50
SD	0.0136	0.0123	0.0122	0.0074
Samples	225	195	170	44
u (m/s)	4	4.5	5	5.5
SD	0.0136	0.0135	0.0129	0.0129
Samples	225	116	56	40
β (degrees)	90	75	60	45
SD	0.0136	0.0135	0.0147	0.0169
Samples	225	157	106	50

5. Transient full-scale measurements

The second type of analysis that was carried out using the NMT data was to study the build up of side force during sudden gust events. The full dataset was interrogated to identify segments of data where the yaw angle increased from near zero to a maximum value of over 5 degrees within two seconds, and then fell to a value near zero. Only data for vehicle speeds greater than 20m/s and wind speeds greater than 4m/s was accepted. This resulted in 220 datasets of lengths varying from 6 to 30 seconds. The geographical location of these data sets and the range of train speeds, wind speeds and wind directions are shown in figure 17. As with the earlier analysis, it can be seen that there is a wide geographical spread of data.

As a first step in the analysis the correlations between the time series of yaw angle and side force coefficient per unit length were calculated. The correlation coefficients are shown in figure 18. It can be seen that the majority of the coefficient are in the range of 0.5 to 1.0, but there are a number that are significantly below this, or even negative. This effect was investigated on a gust-by-gust basis and a small subset of the data is shown in figure 19 for a range of correlation coefficients. This shows the yaw angle and wind time series and a satellite picture of the measurement site. Essentially, the more complex the geometry surrounding the site, the lower the correlation between yaw angle and side force coefficient per unit length. This is of course quite reasonable and illustrates the significant effect of local topography / ground cover on the flow around trains as discussed above. Figure 20 shows a similar figure for three datasets with high correlation coefficients. These can all be seen to be from data obtained at relatively clean rural environments, with the gusts being caused by

the train emerging from localized cover. This is quite consistent with the analysis of the one second gusts presented above.

In the same way as with the earlier analysis, the maximum side force coefficient per unit length measured on the NMT in each gust event can be plotted against the maximum yaw angle in each event. This is shown in figure 21. Figure 21a shows the results for all datasets and the results are similar to those of figure 15, although extend over a rather greater yaw angle range due to maximum rather than average value of yaw angle being used in the figures. There is a noticeable increase in the magnitude of the coefficients for the higher magnitude yaw angles – possibly because of the fact that the Pitot tube will give low values of velocity at these yaw angles, and thus higher values of the coefficients. Figures 21b shows only the data for which the correlation coefficient is greater than 0.7. This shows a better agreement with the wind tunnel data. Finally figure 21c shows a similar result, but for data with a correlation coefficient of greater than 0.9. Here all the outlying data points have been lost, and there is excellent agreement with the wind tunnel data. Note however there are only 42 points plotted in figure 20c i.e. only around 20% of the gust events show a high level of correlation between yaw angle and side force coefficient per unit length around the measurement loop on the NMT. This lack of correlation in most of the data may well explain much of the scatter found in the earlier analysis of one-second values.

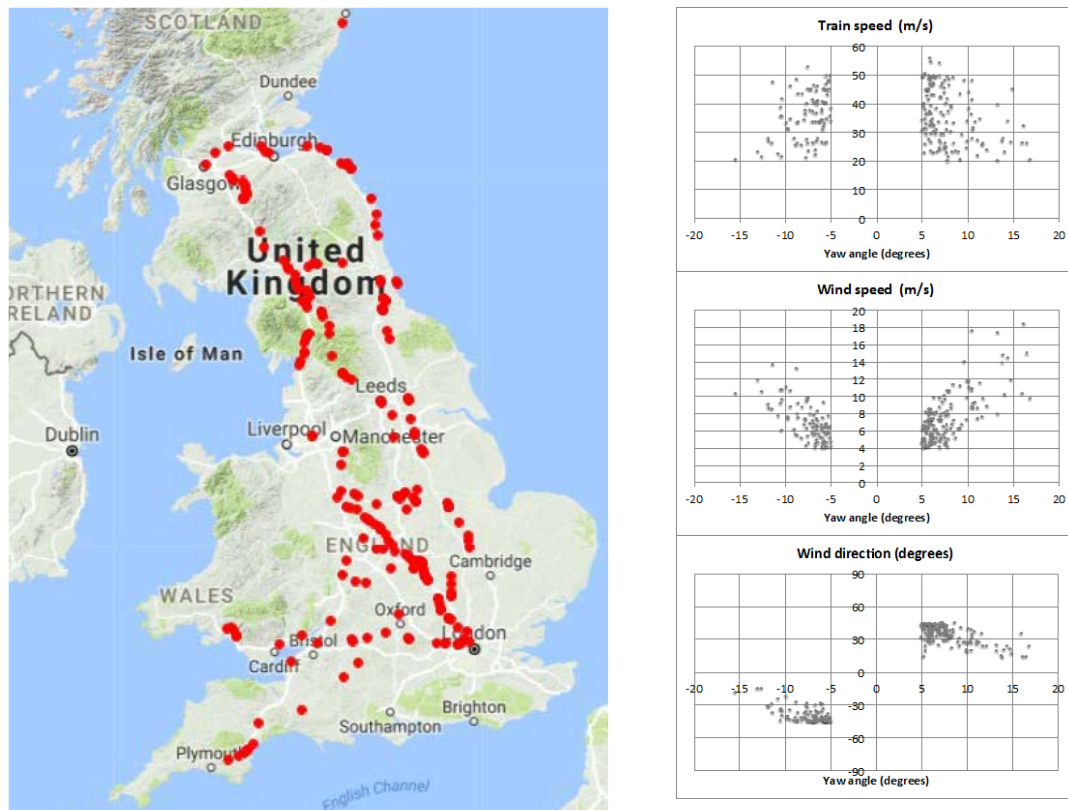
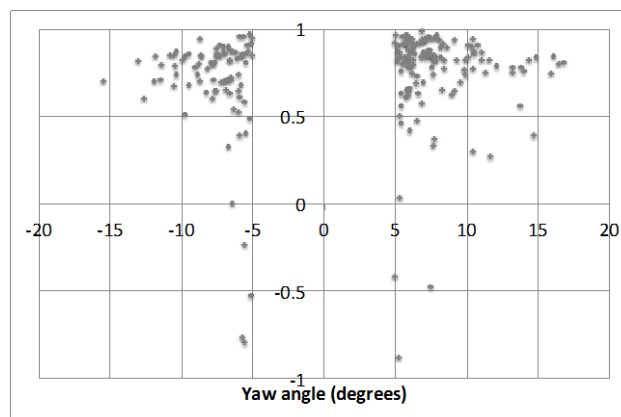


Figure 17 NMT gust measurement locations and conditions for gust analysis (vehicle speed cut off of 20m/s; yaw angle cut off of 5 degrees)

668



669

670

671

Figure 18 Correlation between yaw angle and side force coefficient per unit length time histories for gust analysis datasets.

673

674

675

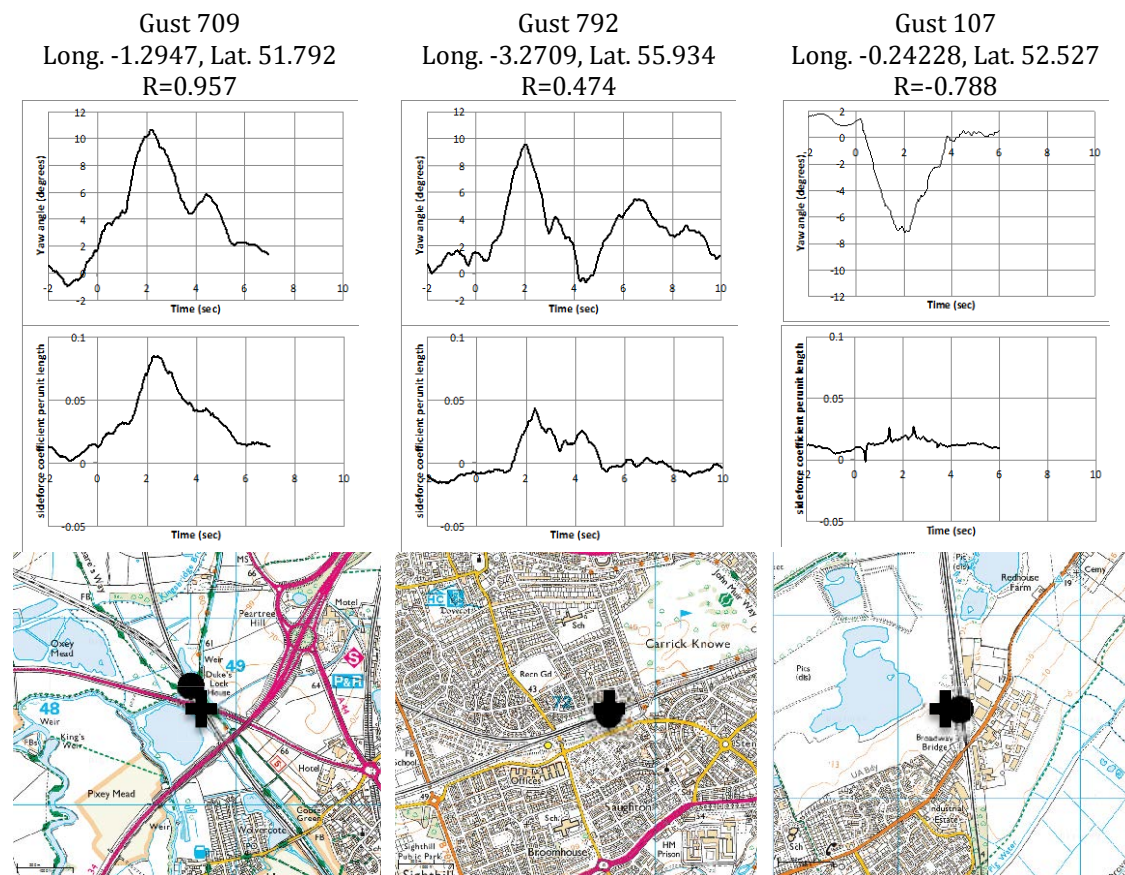


Figure 19 Gusts analysis for a range of correlation coefficients

676
677

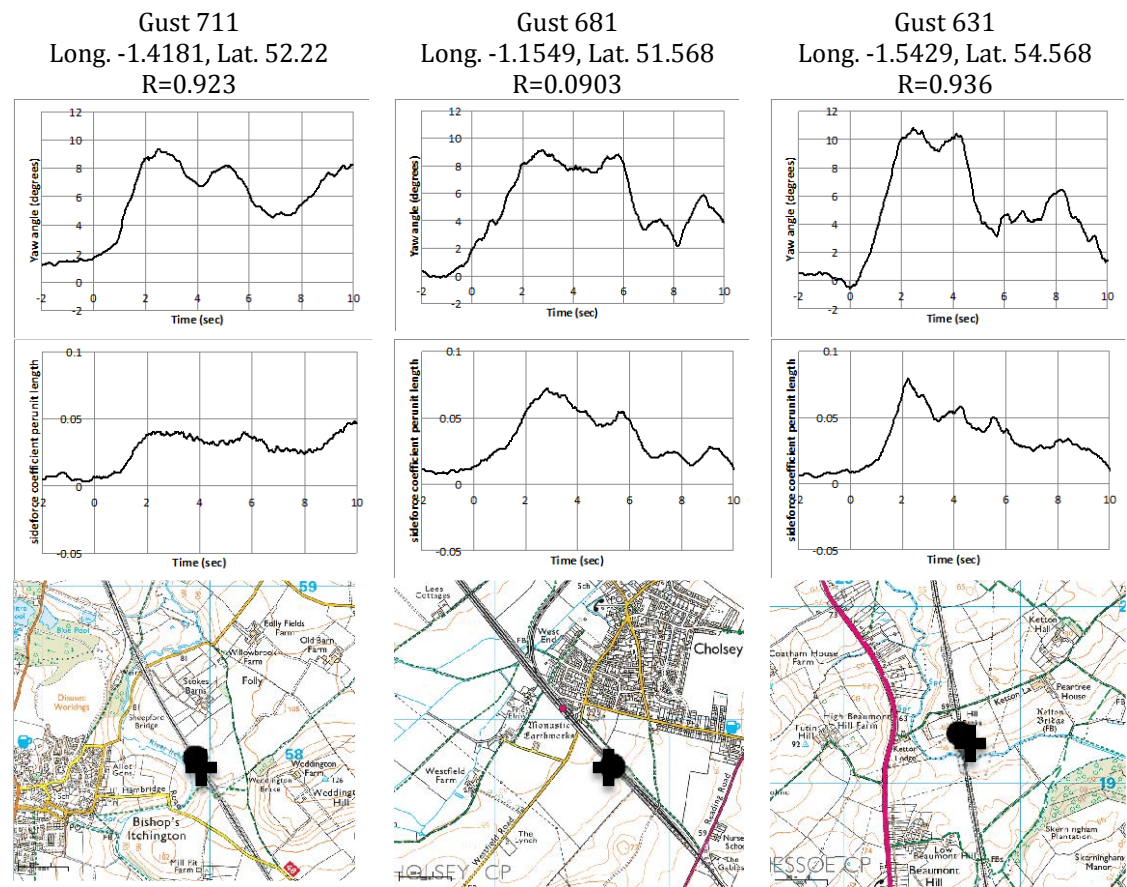
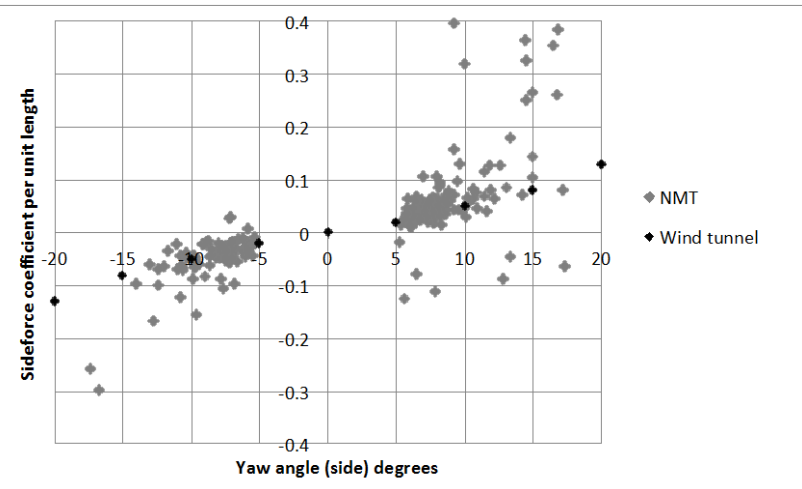


Figure 20 Gust analysis for datasets with high correlation coefficients and yaw angles between 9 and 11 degrees.

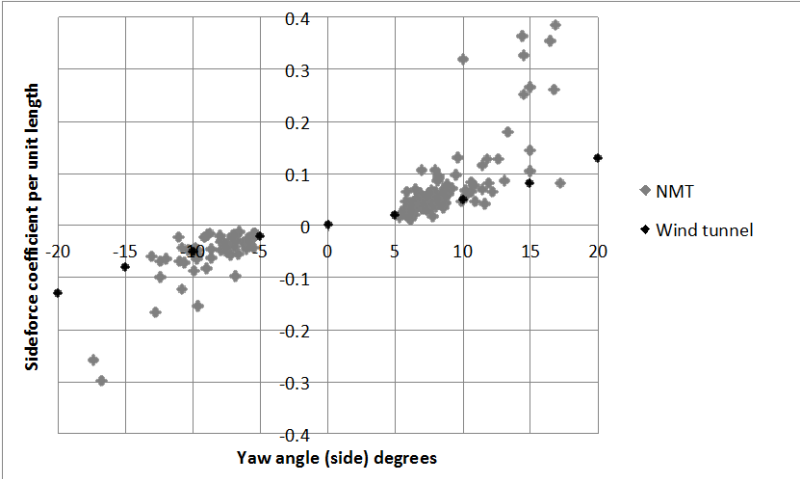
680



681

682

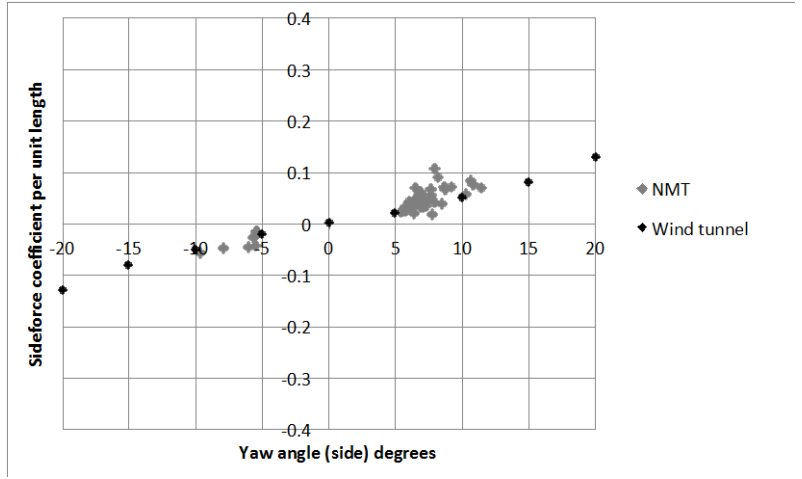
(a) All datasets



683

684

(b) Datasets with $R > 0.7$



685

686

(c) Datasets with $R > 0.9$

687

688

689

Figure 21 Side force coefficient per unit length against yaw angle for different levels of correlation

6. Conclusions

From what has been presented in earlier sections, the following main conclusions can be drawn.

- The flow field around the Class 43 train revealed by CFD calculations and wind tunnel surface pressure measurements, is similar to that that has been measured in the past on other trains, with longitudinal wake vorticity and a suction peak around the nose of the train.
- The two physical modeling measurement techniques (stationary wind tunnel tests and moving model TRAIN Rig tests) and the DDES CFD simulations all give values of the aerodynamic pressure and force coefficients per unit length that are very similar to one another.
- The use of the NMT to obtain full-scale experimental data for cross wind effects has been broadly successful, although the data requires careful analysis to reveal the nature of the flow around the train.
- The analysis of one second gust values of side force coefficient per unit length revealed considerable scatter due to both random unsteadiness in the wind, and also due to the proximity of barriers to the movement of the flow on the near side of the train (such as trees / cuttings etc.). This scatter was much reduced by only using data for high train velocities.
- In general, this analysis showed that the average values of the NMT data and the wind tunnel data (and thus the TRAIN Rig and CFD data) for pressure and side force coefficients are in reasonable agreement, over the rather restricted yaw angle range of the full-scale data.
- An analysis of sudden gust events was carried out. There was a large range of correlation values between the measured yaw angle and side

715 force coefficient time histories. The correlation decreased as the
716 topography around the track became more complex and urbanised. High
717 correlation coefficients occurred when the topography of the surrounding
718 area is simple with few obstructions. For the gust events with high
719 correlations, there was a well-defined side force coefficient with yaw
720 angle curve that lay close to the wind tunnel results.

721 These results strongly suggest that the results of physical and computational
722 modeling techniques, whilst predicting the average values of the force
723 coefficients quite well, should be viewed with some circumspection and can only
724 properly be regarded as an approximation to a highly complex reality.

Acknowledgements

This work was carried out as part of the project “The measurement of train aerodynamic phenomena in operational conditions” funded by the UK Engineering and Physical Sciences Research Council (Grant EP/I03842X/1). The support of a number of colleagues in the Birmingham Centre for Railway Research and Education in developing the data acquisition system is gratefully acknowledged. The project relied on the considerable assistance given by the Network Rail staff who maintain and operate the New Measurement Train, without whom the work described here would simply not have been possible.

References

- Baker C (2013) “A framework for the consideration of the effects of crosswinds on trains”, *Journal of Wind Engineering and Industrial Aerodynamics* 123, 130–142, <http://dx.doi.org/10.1016/j.jweia.2013.09.015>
- Baker C, Sima M, Harwood N, Furio N (2015) “Special Issue: AeroTRAIN and DynoTRAIN projects” *Proceedings of the Institution of Mechanical Engineers. Part F Journal of Rail and Rapid Transit*, 229, 6, 567-569, <http://dx.doi.org/10.1177/0954409715585215>
- CEN (2016) *Railway applications — Aerodynamics — Part 6: Requirements and test procedures for cross wind assessment* prEN 14067-6 2009-02, CEN/TC 256
- Cheli F, Corradi R, Rocchi D, Tomasini G, Maestrini E (2010) “Wind tunnel tests on train scale models to investigate the effect of infrastructure scenario”, *Journal of Wind Engineering and Industrial Aerodynamics* 98, 353-362, <http://dx.doi.org/10.1016/j.jweia.2010.01.001>

749 Cooper R K (1980) "The probability of trains overturning in high winds",
 750 Proceedings of the 5th International Conference on Wind Engineering, editor
 751 Cermak J, 2, 1185-1194
 752 Dorigatti F (2013) "Rail vehicles in crosswinds: analysis of steady and unsteady
 753 aerodynamic effects through static and moving model tests", University of
 754 Birmingham PhD thesis, <http://etheses.bham.ac.uk/4267/>
 755 Dorigatti F, Sterling M, Baker C, Quinn A (2015) "Crosswind effects on the
 756 stability of a model passenger trains - comparison of static and moving
 757 experiments", Journal of Wind Engineering and Industrial Aerodynamics 138,
 758 36-51, <http://dx.doi.org/10.1016/j.jweia.2014.11.009>
 759 Eichinger S, Sima M, Thiele F (2015) "Numerical simulation of a regional train in
 760 cross-wind", Proceedings of the Institution of Mechanical Engineers. Part F
 761 Journal of Rail and Rapid Transit 229, 6, 625- 634
 762 <http://dx.doi.org/10.1177/0954409714555383>
 763 Gallagher M (2016) "Experimental Investigation of the Aerodynamics of a Class
 764 43 High Speed Train", PhD Thesis, University of Birmingham,
 765 <http://etheses.bham.ac.uk/7269/>
 766 Ko Y-Y, Chen C-H, Hoe I-T, Wang S-T (2012) "Field measurements of
 767 aerodynamic pressures in tunnels induced by high speed trains", Journal of Wind
 768 Engineering and Industrial Aerodynamics 100, 19- 29
 769 <http://dx.doi.org/10.1016/j.jweia.2011.10.008>
 770 Matschke G, Heine C (2002) "Full-scale tests on side wind effects on trains –
 771 evaluation of aerodynamic coefficients and efficiency of wind breaking devices",
 772 in "TRANSAERO – A European initiative on transient aerodynamics for railway
 773 system operation" editors Schulte-Werning B, Gregoire R, Malfatti A, Matschke G,

774 Notes on numerical fluid dynamics and multi-disciplinary design – 79, 27-38,
 775 Springer
 776 Mair W A, Stewart A J (1985) “The flow past yawed slender bodies, with and
 777 without ground effects”, Journal of Wind Engineering and Industrial
 778 Aerodynamics 18, 3, 301-328, [https://doi.org/10.1016/0167-6105\(85\)90088-1](https://doi.org/10.1016/0167-6105(85)90088-1)
 779 Morden J (2016) “A numerical investigation of the effects of crosswinds upon the
 780 aerodynamic characteristics of a high speed passenger train and its slipstream”,
 781 PhD Thesis, University of Birmingham, <http://etheses.bham.ac.uk/7188/>
 782 Morden J, Hemida H, Baker C (2015) “A comparison of RANS and Detached Eddy
 783 Simulation Results to Wind-Tunnel Data for the Surface Pressures Upon a Class
 784 43 High-Speed Train”, ASME Journal of Fluids Engineering 137, 4, 41108 FE-14-
 785 1185, <http://dx.doi.org/10.1115/1.4029261>
 786 OpenFOAM, 2014; Online: <http://openfoam.com> (last visited 01/12/2017)
 787 Quinn A D, Sterling M, Robertson A P, and Baker C J (2008) “An Investigation of
 788 the wind induced rolling moment on a commercial vehicle in the atmospheric
 789 boundary layer”, Proceedings of the I.Mech.E Part D, Journal of Automobile
 790 Engineering 221, 1367-1379, <http://dx.doi.org/10.1243/09544070JAUTO537>
 791 RAPIDE consortium (2001) Final Report - Railway Aerodynamics for Passing
 792 and Interaction with Dynamic effects, 6R / 011030-1 / EA
 793 Richardson G M, Hoxey R P, Robertson A P, Short J L (1995) “The Silsoe
 794 Structures Building: The Completed Experiment Part 1”, 9th International
 795 Conference on Wind Engineering, Wind Engineering retrospect and prospect;
 796 New Delhi
 797 Soper D, Gallagher M, Baker C, Quinn A (2016), A model-scale study to assess the
 798 influence of ground geometries on aerodynamic flow development around a

799 train, Proceedings of the Institution of Mechanical Engineers, Part F: Journal of
800 Rail and Rapid Transit <http://dx.doi:10.1177/0954409716648719>
801 Soper D, Baker C, Jackson A, Milne D, Le Pen L, Watson G, Powrie W (2017) Full-
802 scale measurements of train underbody flows and track forces, Journal of Wind
803 Engineering and Industrial Aerodynamics 169, 251-264,
804 <http://dx.doi.org/10.1016/j.jweia.2017.07.023>
805 Sturt R, Baker C, Soper D, Vardy A, Howard M, Rawlings C (2015) “The Design of
806 HS2 tunnel entrance hoods to prevent sonic booms”, Railway Engineering
807 Conference, Edinburgh
808 Vardy A, Sturt R, Baker C and Soper D (2015) “The behaviour of long entrance
809 hoods for high speed rail tunnels” ISAVFT-2005 Paper-1